LA-UR- 11-04947

Approved for public release; distribution is unlimited.

Title:	Turbulence and Mixing Characteristics in the Variable Density Rayleigh-Taylor Mixing Layer
Author(s):	D. Livescu, M.R. Petersen, T. Wei
Intended for:	Third International Conference "Turbulent Mixing and Beyond," Trieste, Italy, 08/21-08/27 2011

Los Alamos
NATIONAL LABORATORY
EST. 1943

Form 836 (7/06)

Turbulence and mixing characteristics in the variable density Rayleigh-Taylor mixing layer

Daniel Livescu, Mark Petersen and Tie Wei

CCS-2 Los Alamos National Laboratory

Acknowledgements: Rob Gore, Malcolm Andrews, Ray Ristorcelli

Turbulence and mixing characteristics in the variable density Rayleigh-Taylor mixing layer

Objectives

- **Present a new set of very large, fully resolved simulations of Rayleigh-Taylor instability.**
- **Examine the turbulence characteristics at high Reynolds numbers in the variable-density Rayleigh-Taylor layer.**

Problem description: Rayleigh-Taylor instability

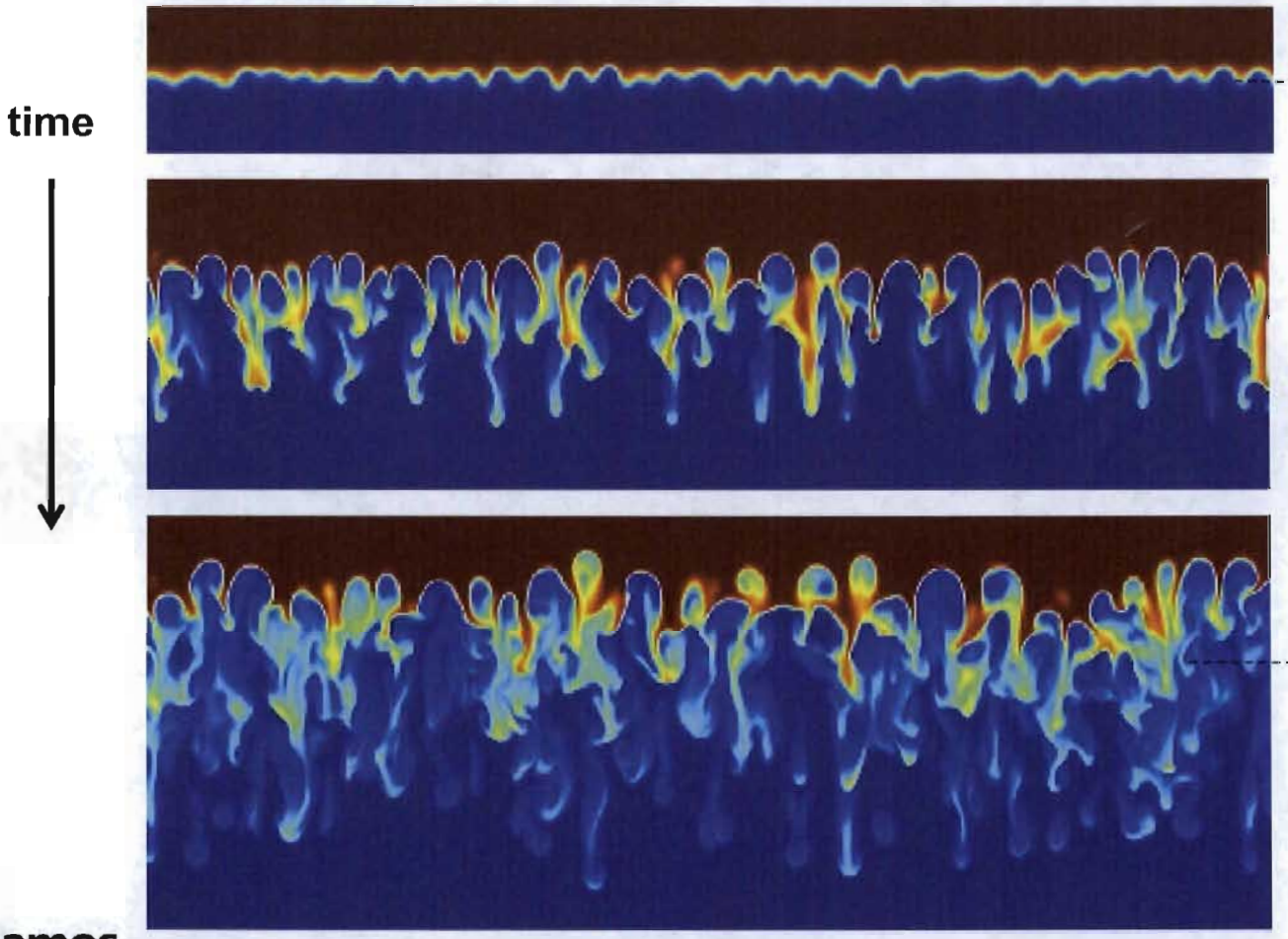

Buoyancy-driven instabilities

Supernova

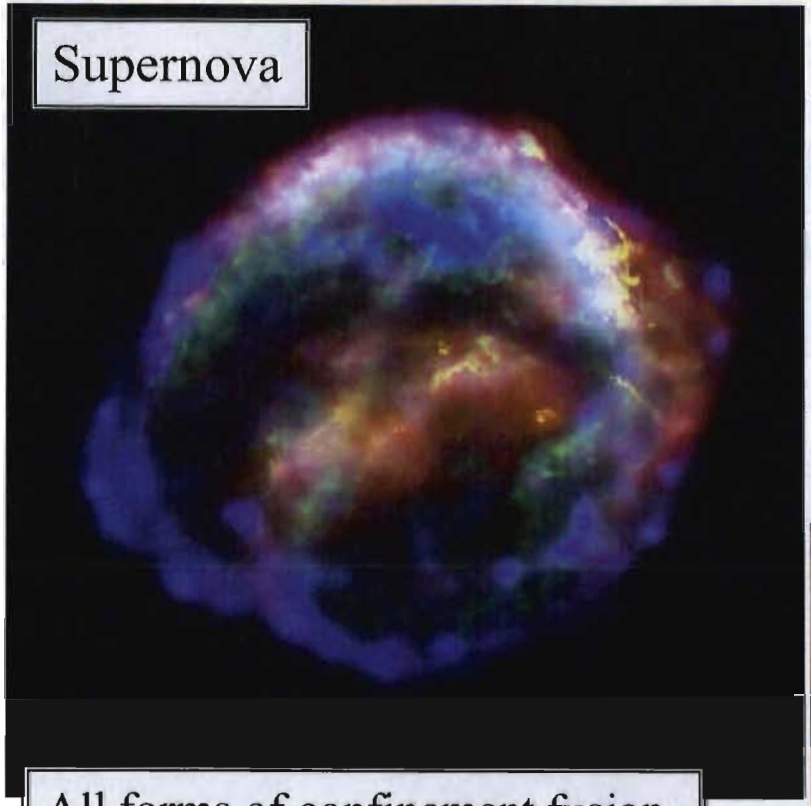

Mammatus clouds

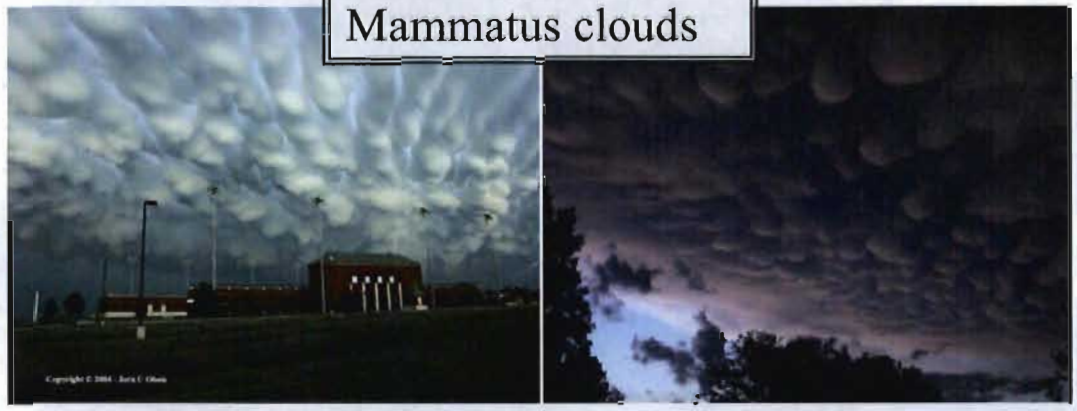

ICF target

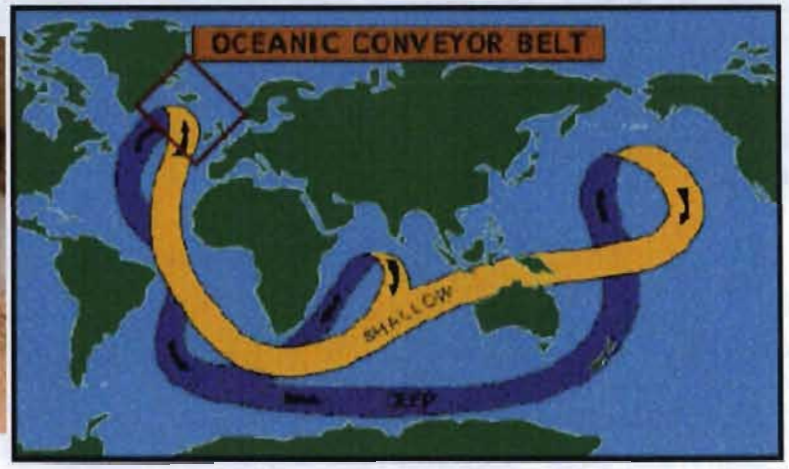

All forms of confinement fusion (gravitational, magnetic, inertial)

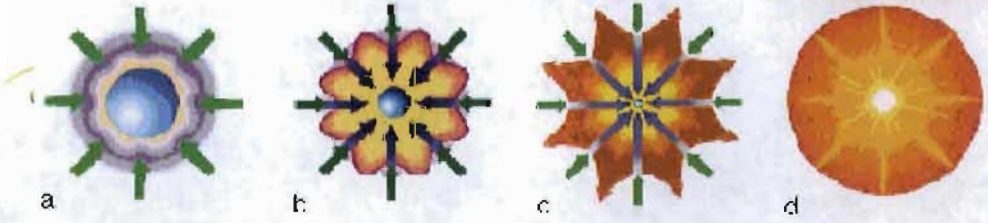

ED

NNSA

Other examples of buoyancy-driven instabilities

From a brief literature search:

- All astrophysical explosions (e.g. X-Ray bursts or giant flares).
- Sonoluminescence.
- Industrial coating with thin liquid films.
- Sound generation by snapping shrimp due to the collapse of cavitation bubbles.

Current problems in RTI

- Although RTI has been studied over the last 60 years, until recently, most studies have been focused on the layer growth rate and the discrepancy between the experimental and numerical growth rates.
- Recent advances in computer power and experimental techniques have lead to increased understanding of RTI however, compared to other canonical turbulent flows, not much is known beyond low order moments. Examples where our knowledge is particularly lagging:
  - Turbulence spectral dynamics and intermittency
  - Mixing characteristics (including A dependence)
  - Instability front properties
  - Role of initial conditions
- Main difficulties:
  - initial conditions control and diagnostics in experiments
  - very large meshes required for accurate numerical simulations

Variable-density buoyancy-driven turbulence

- **Mixing between fluids with very different densities: variable-density mixing.**
- **The equations describing the variable-density mixing between two incompressible fluids can be derived from the compressible Navier-Stokes equations with two ideal gases, by letting $P, T \rightarrow \infty$ such that $\rho_1 = P/(T\,\mathbf{R}\,W_1)$ and $\rho_2 = P/(T\,\mathbf{R}\,W_2)$ remain constant.**

Continuity $$\rho_{,t} + (\rho u_j)_{,j} = 0$$

Momentum $$(\rho u_i)_{,t} + (\rho u_i u_j)_{,j} = -p_{,i} + \mu(u_{i,j} + u_{j,i} - 2/3\delta_{ij}u_{k,k})_{,j} + \rho g_i$$

Divergence condition $$u_{j,j} = -\mathbf{D}\,Ln(\rho)_{,jj}$$

Direct Numerical Simulations of variable-density mixing

- **Code used: CFDNS (Livescu et al LA-CC-09-100).**
- **For this problem, mixed FFTs - 6th order compact finite differences.**
- **Main difficulty: Density variations lead to a variable coefficient Poisson equation (Livescu and Ristorcelli, J. Fluid Mech. 2007).**
  - Closed form solution for the gradient component of $\nabla p/\rho$, responsible for mass conservation
  - Iterative solver for the curl component of $\nabla p/\rho$, related to the baroclinic production of vorticity (Livescu and Ristiorcelli, J. Fluid Mech. 2007 and Chung and Pullin, J. Fluid Mech. 2010).
- **Extensive resolution studies performed to ensure the accuracy and convergence of the solution.**
- **2-D simulations (up to $16{,}384^2$) performed at LANL and on Jaguar, ORNL.**
- **3-D simulations (up to $4096^2 \times 4032$) performed on Dawn, LLNL; Jaguar, ORNL; and LANL.**

Problem description: new suite of Direct Numerical Simulations of Rayleigh-Taylor instability

- Suite of 1024^2 x 4608 simulations at A=0.04, 0.5, 0.75, 0.9:
  - Base simulations with initial perturbation peaked around the most unstable mode of the linear problem.
  - After the layer width had developed substantially, the simulations were branched into reversed (g -> -g) and zero (g -> 0) gravity simulations.
  - Different initial perturbation spectra, viscosity and diffusion coefficients to study the effects of various parameters.

- 4096^2 x Nz simulation at A=0.75 (NZ_{max}=4032).

- These have reached Reynolds numbers of:

$$\mathrm{Re}_b = h\dot{h}/\nu > 40{,}000$$

$$\mathrm{Re}_T = \tilde{k}^2/\nu\varepsilon > 5500$$

Multi-mode Rayleigh-Taylor instability: A=0.75, grid size 4096^2 x4032

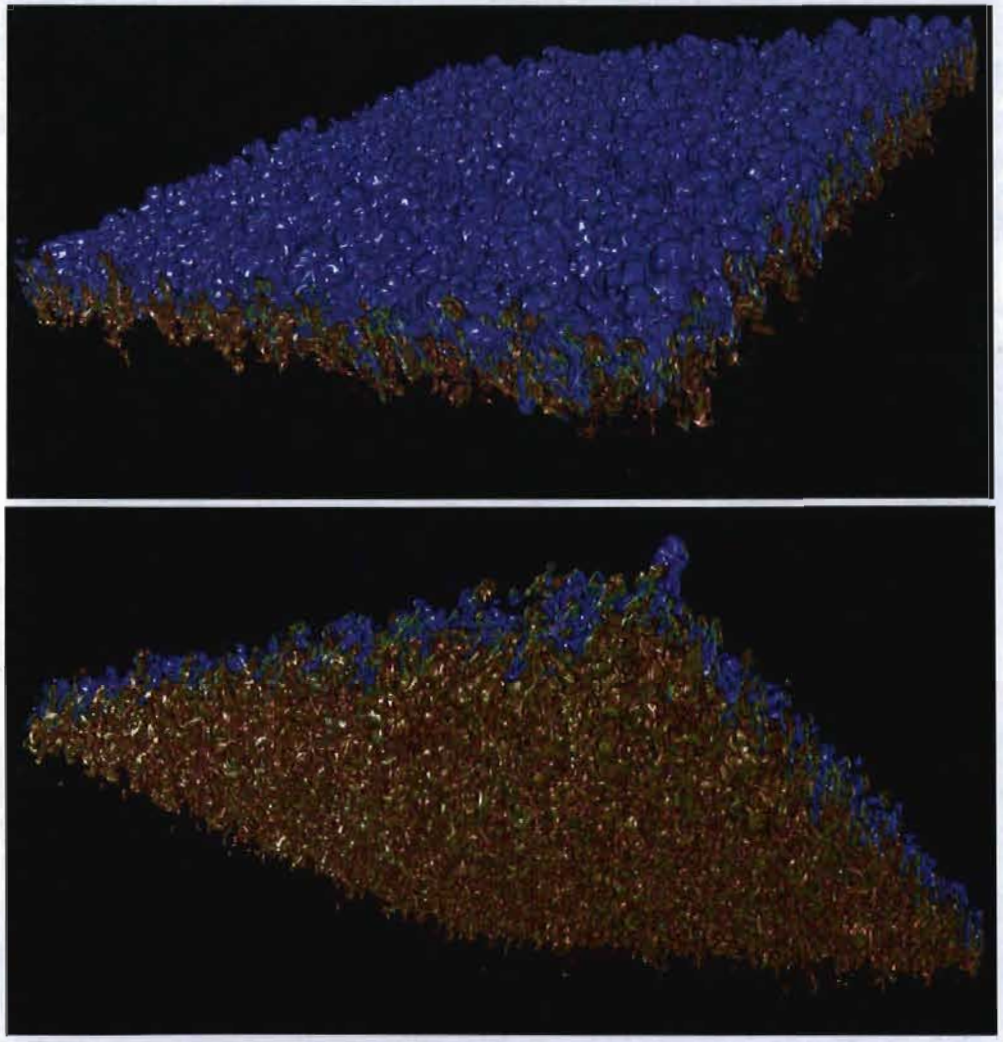

Global measures: mixing layer growth

- **Ristorcelli & Clark, (2004) and Cook et al. (2004) showed that self-similarity of the layer width leads to the solution**

$$h(t) = \alpha A g t^2 + 2\left(\alpha A g h_0\right)^{1/2} t + h_0$$

- **Cabot and Cook (2006) measure** $\alpha = \dot{h}^2 / 4Agh$
- **We introduce a smoother variation that avoids derivatives (left).**
- **David Youngs uses an integral mix measure,** h_{DY} **, to define** α_{DY} **(right).**

$$\alpha = \frac{\left(\sqrt{h_{0.01}(t)} - \sqrt{h_{0.01}(t_0)}\right)^2}{Ag\left(t - t_0\right)^2} \qquad \alpha_{DY} = \frac{\dot{h}_{DY}{}^2}{4Agh_{DY}}$$

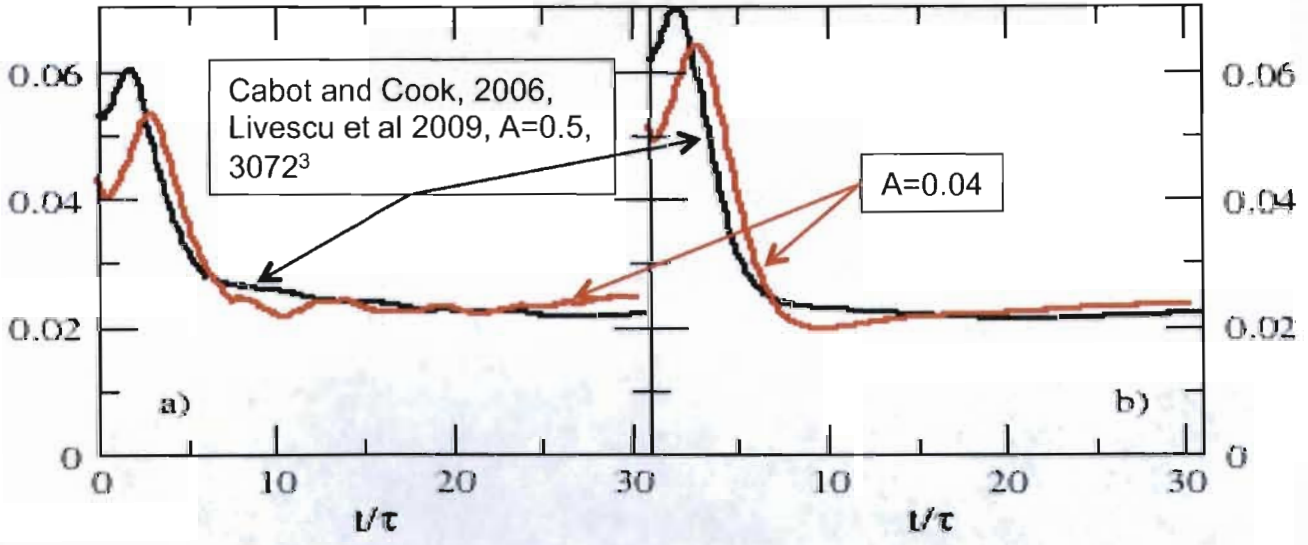

$\tau = \sqrt{L_0 / (Ag)}$

L_0= characteristic lengthscale of the initial perturbation

Global measures: mixing layer growth for different perturbation spectra

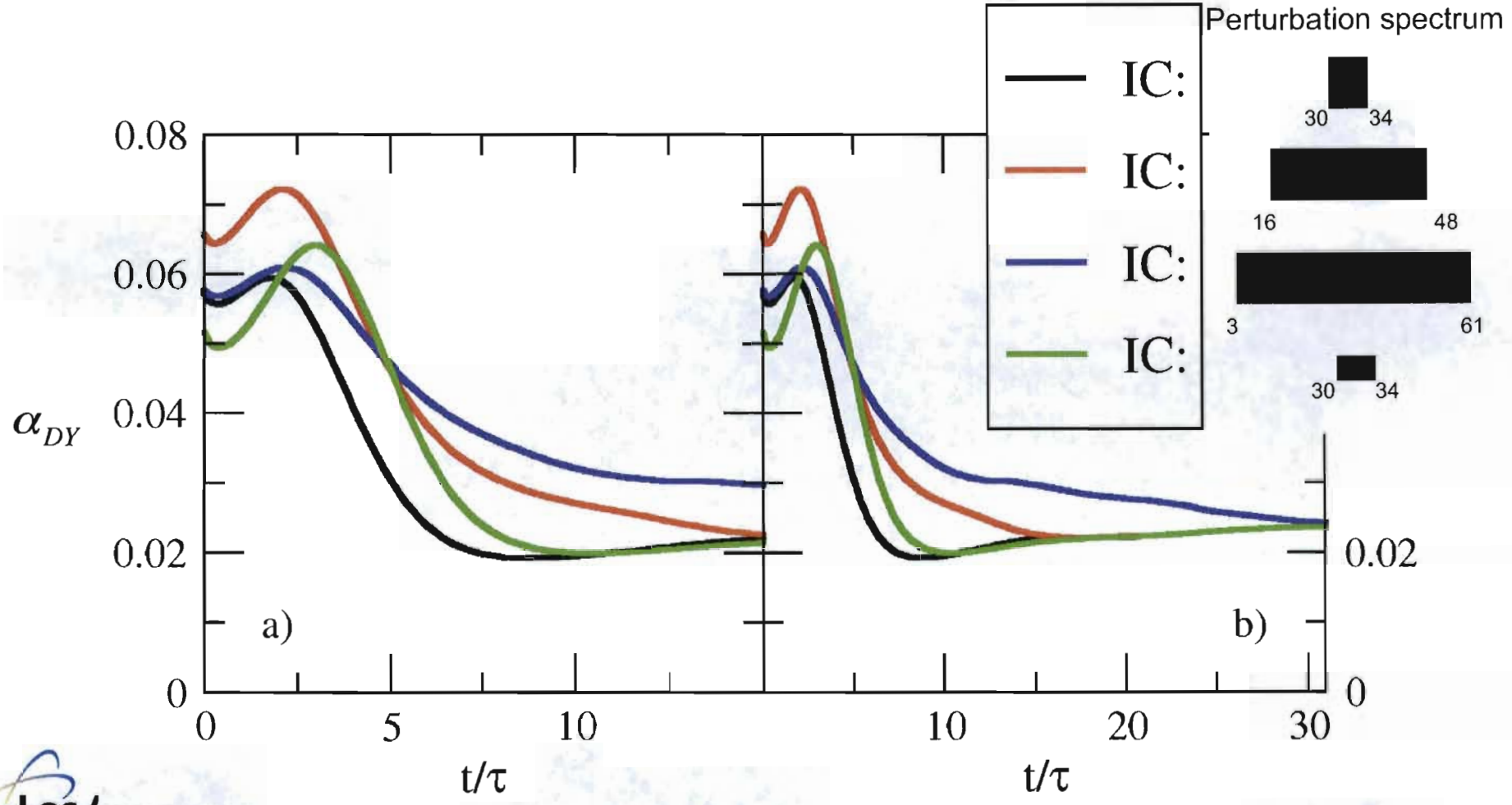

Effects of initial conditions: Rocket-Rig experiments

Rocket-Rig: Expt3-45

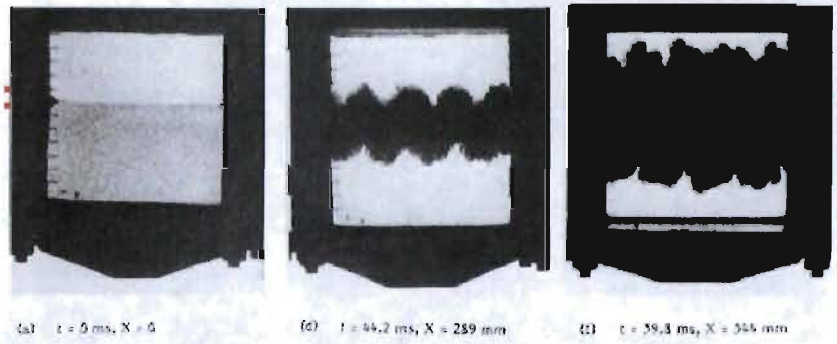

(a) t = 0 ms, X = 0 (d) t = 44.2 ms, X = 289 mm (f) t = 59.8 ms, X = 366 mm

Rocket-Rig: Expt-35

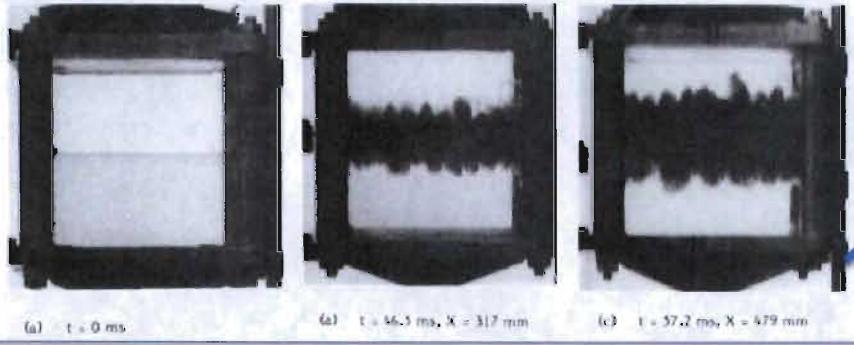

(a) t = 0 ms (d) t = 46.5 ms, X = 317 mm (f) t = 57.2 ms, X = 479 mm

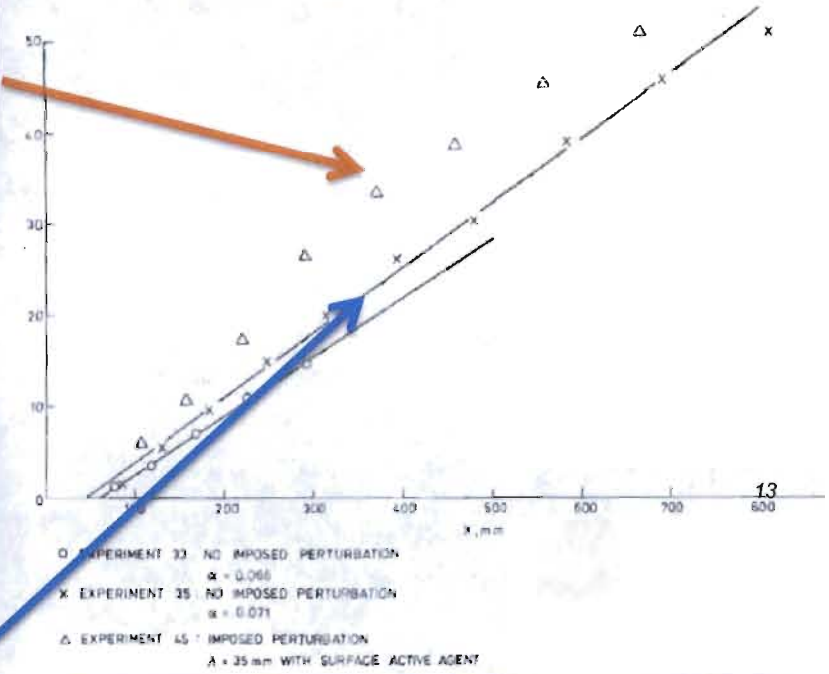

"... in this set (45), a perturbation of unknown origin with a wavelength of about 35mm appeared at the beginning of the experiment. The initial amplitude could not be measured."

Open question:

Effect of initial conditions on mixing layer growth rate, especially at late time.

Effects of initial conditions: membrane separated fluids

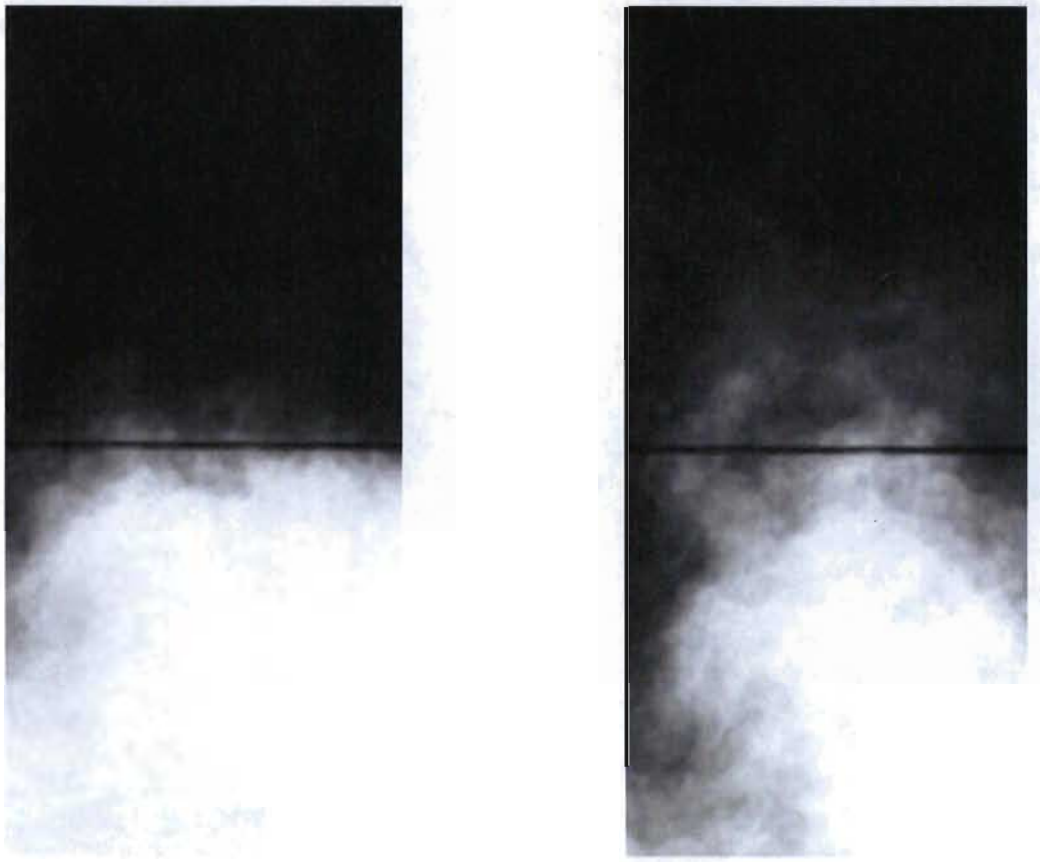

• Rayleigh-Taylor mixing layer resulting initial conditions generating from a retracting membrane (courtesy of A. Banerjee).

Global measures: mixing layer growth for different perturbation spectra

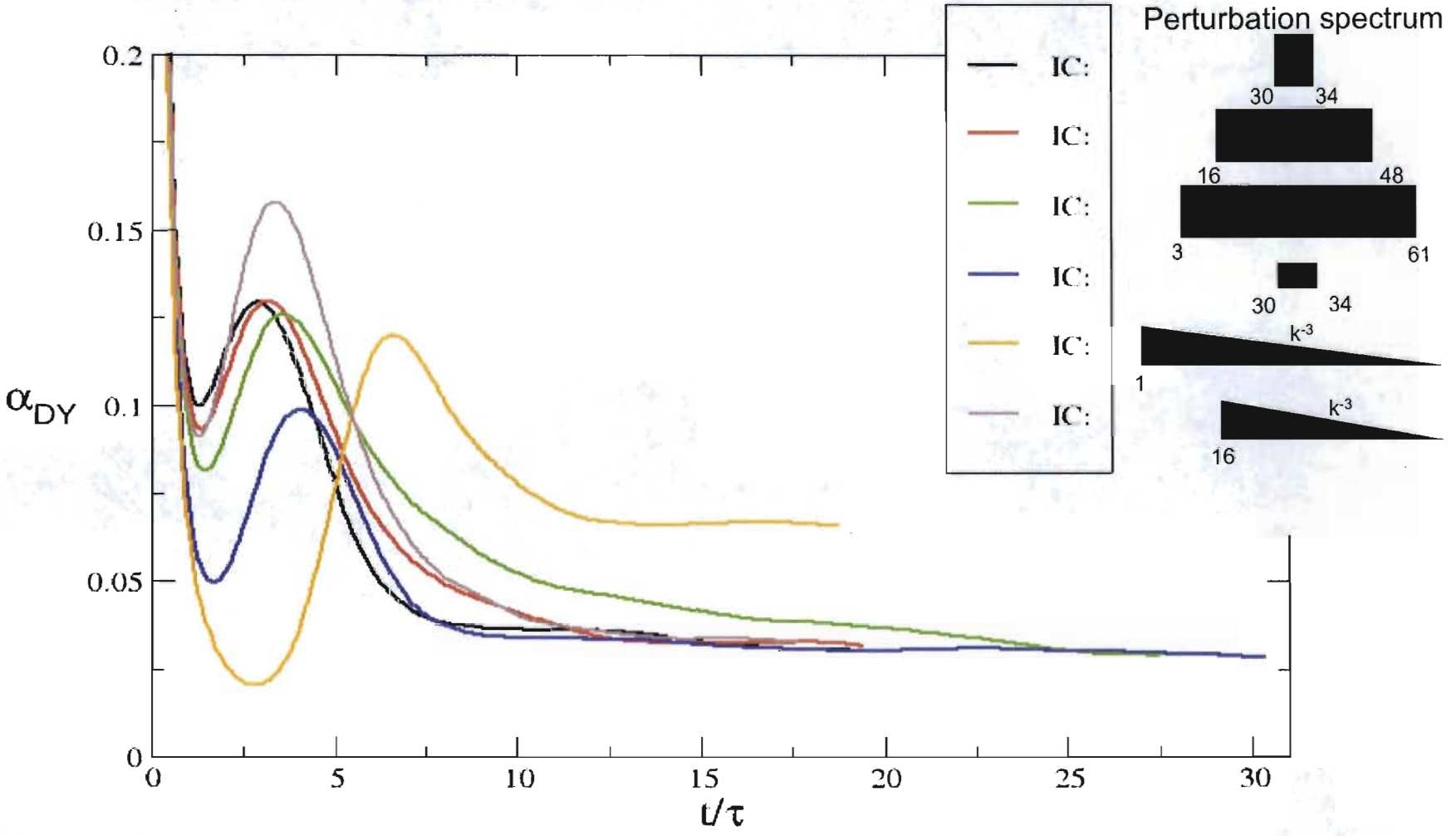

Single-mode RTI: Beyond the "terminal velocity"

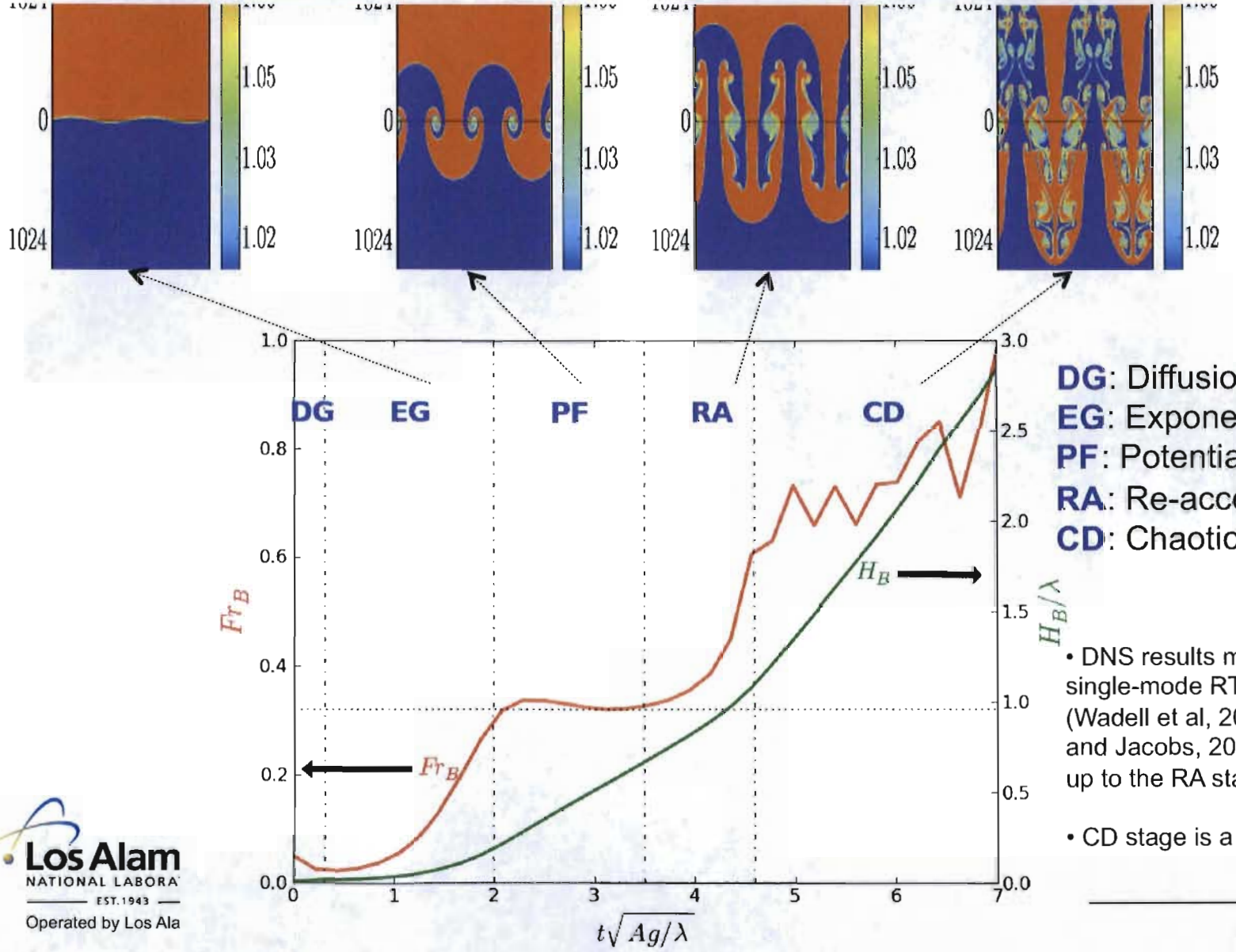

DG: Diffusional growth
EG: Exponential growth
PF: Potential flow
RA: Re-acceleration
CD: Chaotic development

- DNS results match the available single-mode RTI experiments (Wadell et al, 2001, and Willkinson and Jacobs, 2007) which extend up to the RA stage.
- CD stage is a new finding.

Los Alam
NATIONAL LABORA
EST. 1943
Operated by Los Ala

NNSA

Single-mode RTI: Beyond the "terminal velocity"

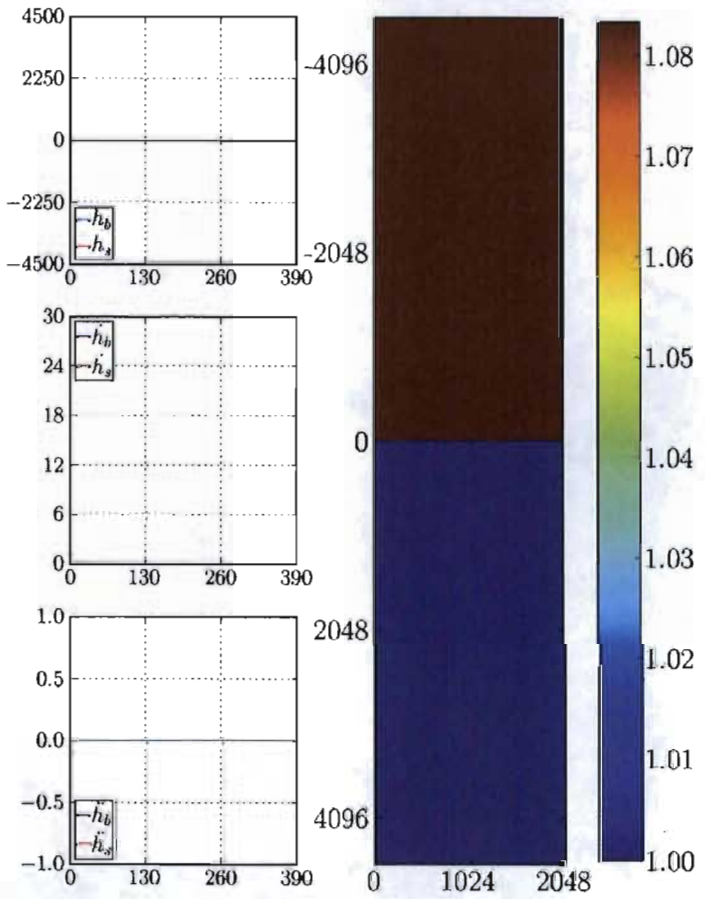

Multi-mode RTI with k^{-3} initial perturbation spectrum, A=0.04

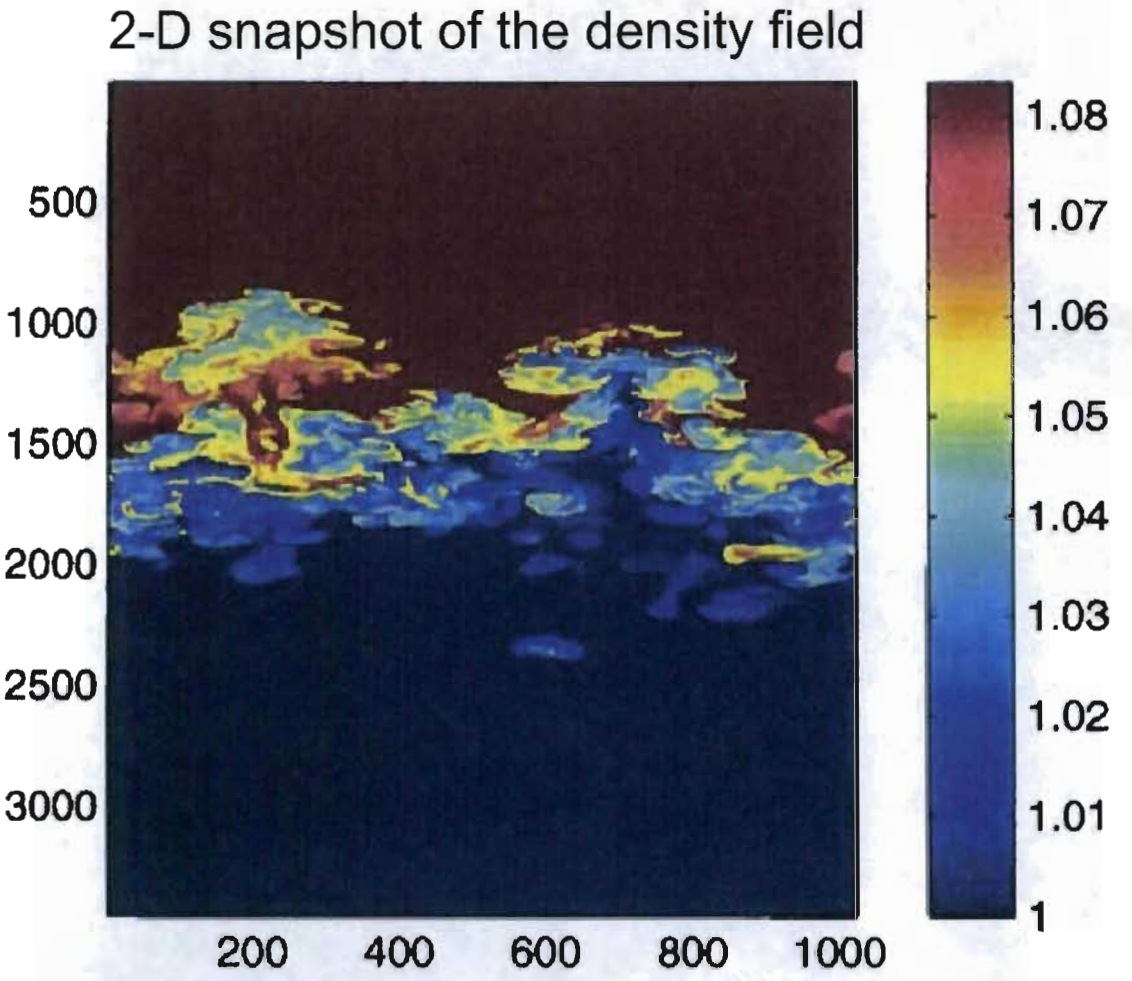

Multi-mode RTI with k^{-3} initial perturbation spectrum, A=0.04

PDFs of the cosine of the angles between the vorticity vector and the eigenvectors of the strain rate tensor corresponding to the eigenvalues α, β, γ, with $\alpha>\beta>\gamma$ ($\alpha>0$, $\gamma<0$).

a) Middle of the layer: alignment with the intermediate eigenvector

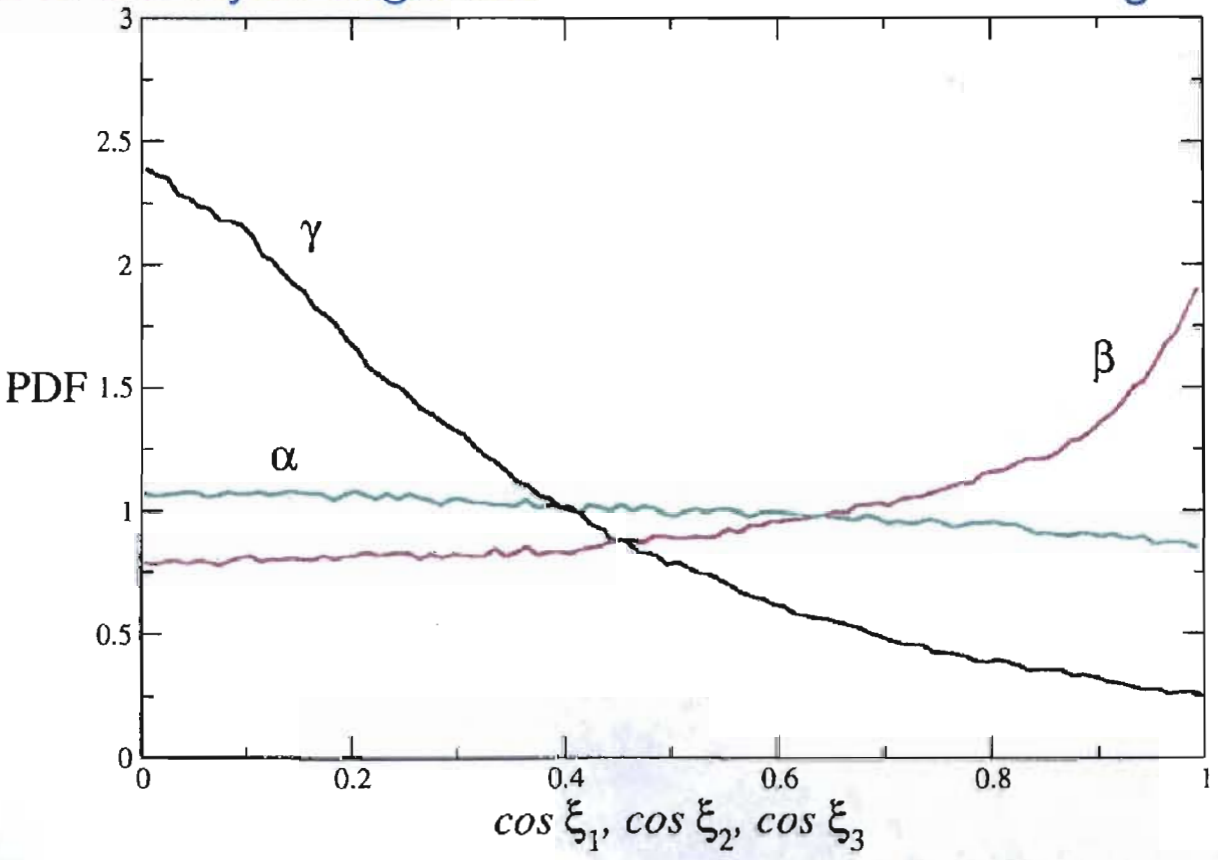

Multi-mode RTI with k^{-3} initial perturbation spectrum, A=0.04

PDFs of the cosine of the angles between the vorticity vector and the eigenvectors of the strain rate tensor corresponding to the eigenvalues α, β, γ, with $\alpha>\beta>\gamma$ ($\alpha>0$, $\gamma<0$).

b) Edge of the layer: alignment almost perpendicular to the α-eigenvector

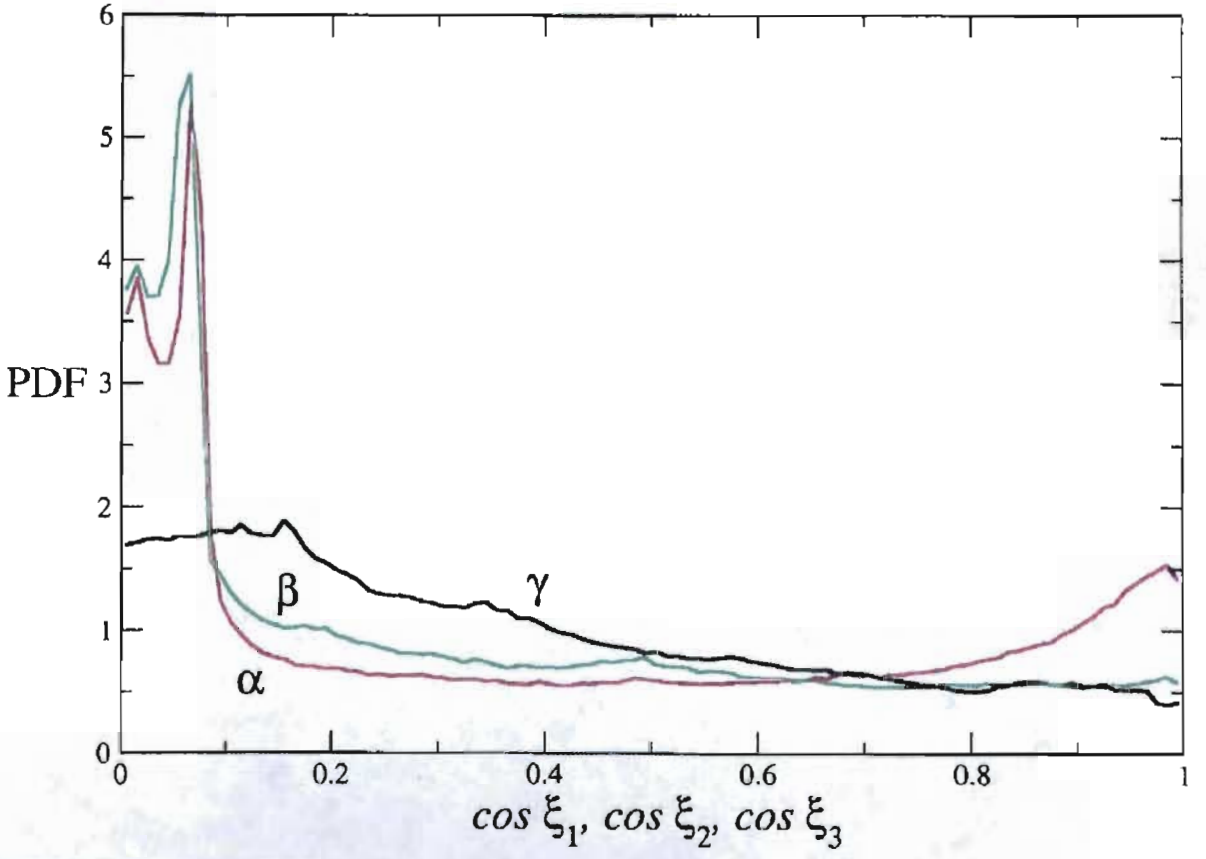

Multi-mode RTI with k^{-3} initial perturbation spectrum, A=0.04

- At the edge of the layer, the α-eigenvector is oriented along the vertical axes of the bubbles / spikes due to the stretching produced by gravity.

- Symmetry conditions prevent the alignment between the vorticity and the α-eigenvector at the edge of the layer, when a dominant mode with wavenumber k=1 is present .

- The alignment of vorticity in planes perpendicular to the α-eigenvector produces induced velocity (and ejections) in the vertical direction, enhancing the growth rate.

Multi-mode RTI, initial perturbation spectrum peaked at high wavenumbers, A=0.75, grid size 4096^2 x4032

2-D snapshot of the density field

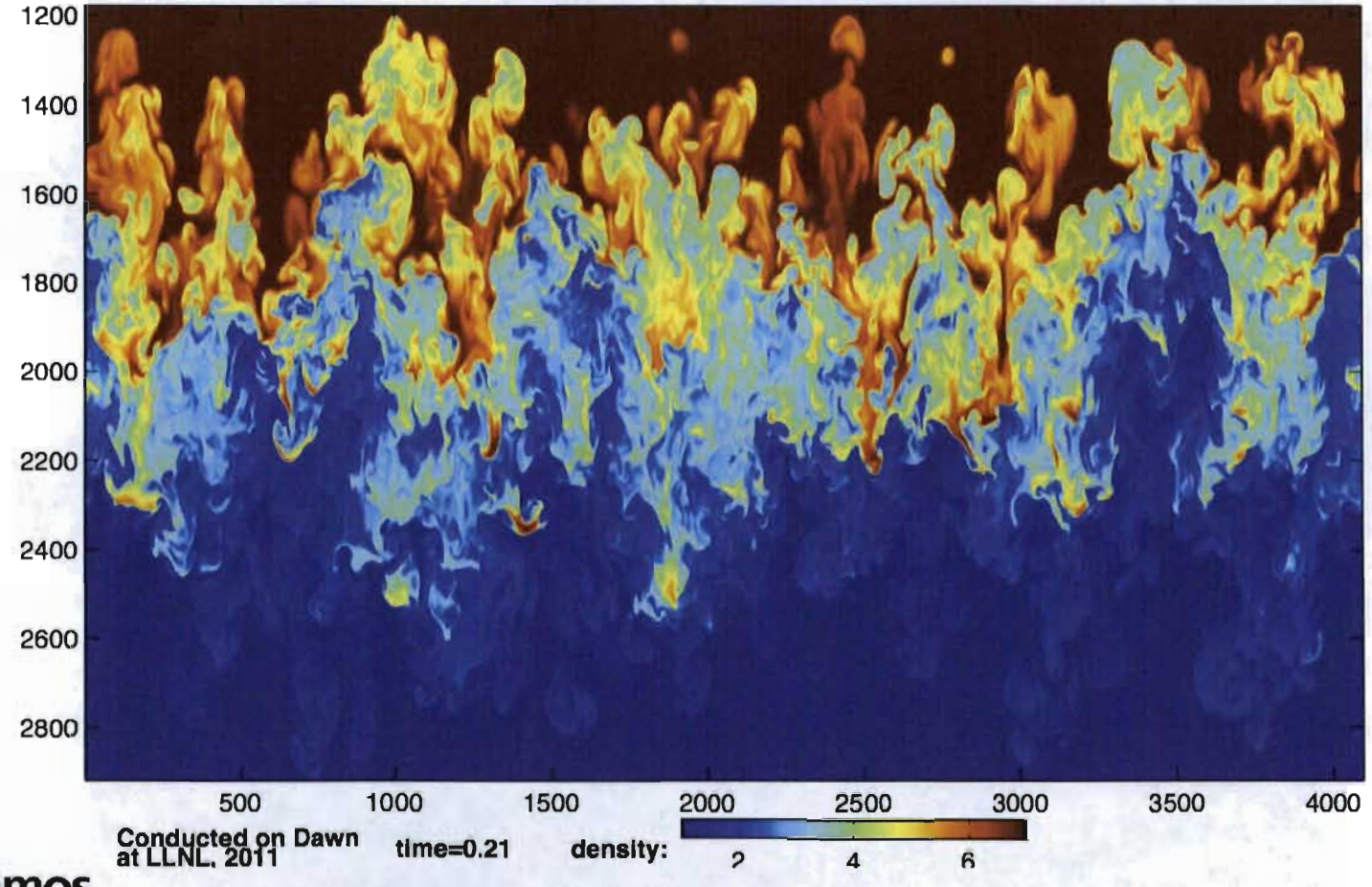

Multi-mode RTI with initial perturbation spectrum peaked at high wavenumbers, A=0.75

PDFs of the cosine of the angles between the vorticity vector and the eigenvectors of the strain rate tensor corresponding to the eigenvalues α, β, γ, with $\alpha>\beta>\gamma$ ($\alpha>0$, $\gamma<0$).

a) Middle of the layer: alignment with the intermediate eigenvector

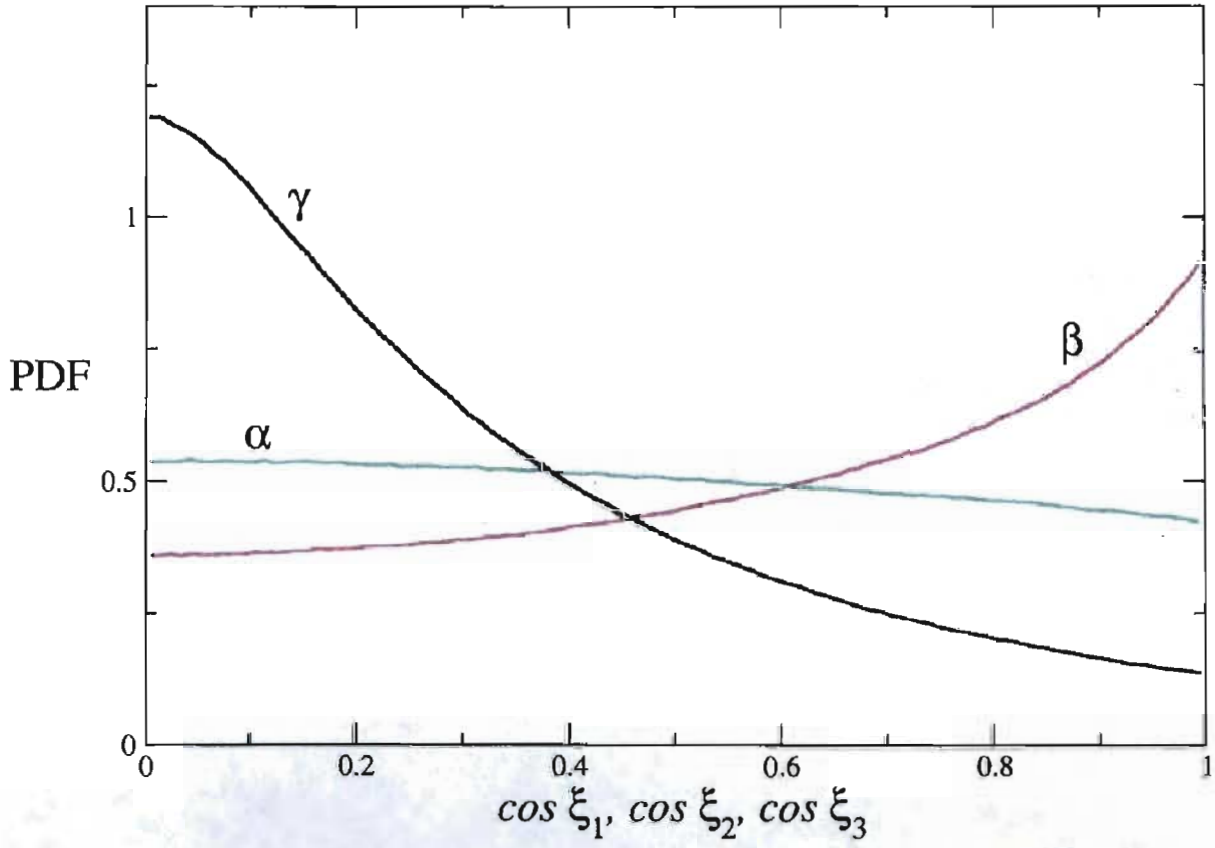

Multi-mode RTI with initial perturbation spectrum peaked at high wavenumbers, A=0.75

PDFs of the cosine of the angles between the vorticity vector and the eigenvectors of the strain rate tensor corresponding to the eigenvalues α, β, γ, with $\alpha>\beta>\gamma$ ($\alpha>0$, $\gamma<0$).

a) Edges of the layer: alignment perpendicular to the α-eigenvector on the spike side.

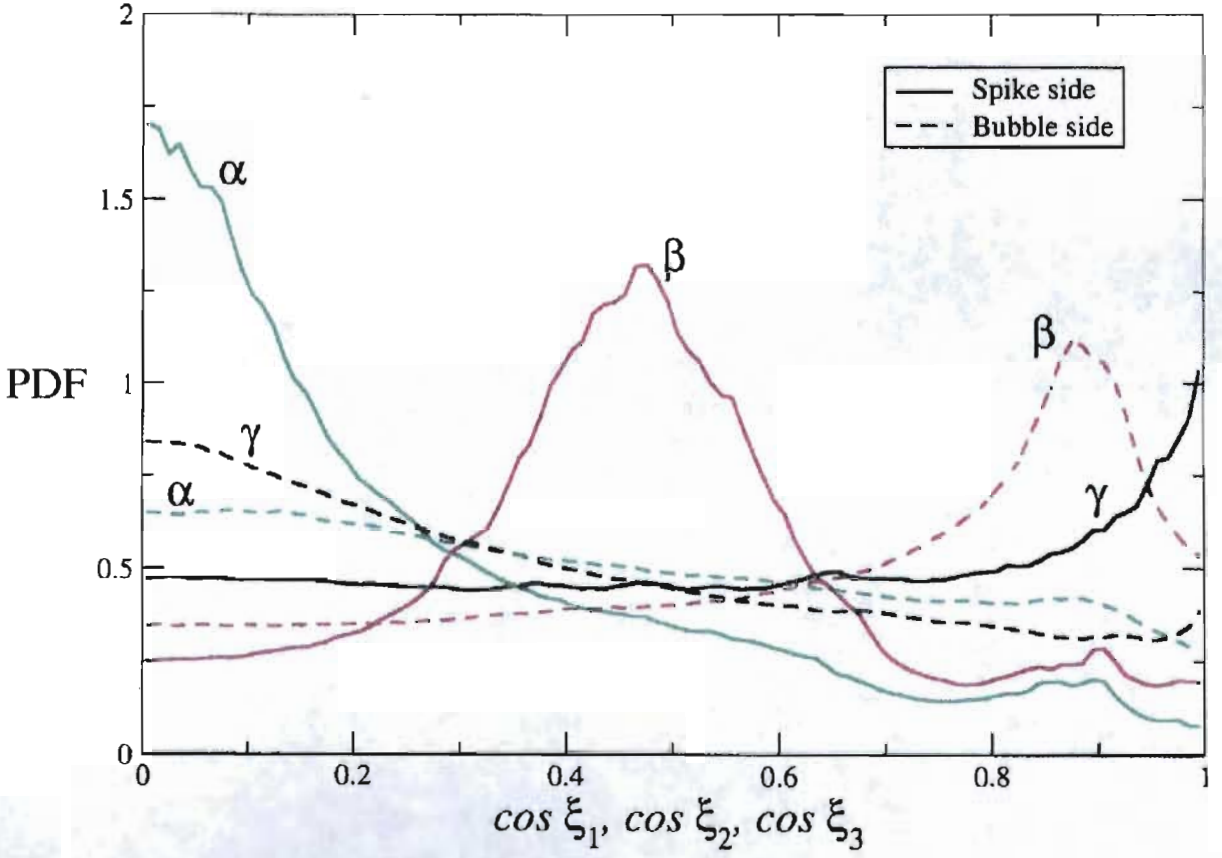

Multi-mode RTI with initial perturbation spectrum peaked at high wavenumbers, A=0.75

Evolution equation for the cosine of the angles between a vorticity element and the principal axes (Boratav et al, Phys. Fluids 1996):

$$\frac{d}{dt}\vec{\Omega} = \begin{pmatrix} \alpha-\Delta & 0 & 0 \\ 0 & \beta-\Delta & 0 \\ 0 & 0 & \gamma-\Delta \end{pmatrix} \vec{\Omega} - \xi_{vorticity}\,\vec{\Omega} - \vec{\Omega'} \mathrm{x} \vec{\Omega} + \bar{B}$$

$\vec{\Omega}$ = vorticity vector in strain coordinates

$\vec{\Omega'}$ = strain rotation vector

$\xi_{vorticity}$ = vorticity stretching rate

$\vec{B}$ = unit baroclinic term projected on strain coordinates

- The baroclinic term becomes large at high A on the spike side.
- This term opposes the alignment with the α-eigenvector so that the vorticity lies in planes perpendicular to the α-eigenvector.
- Again, this produces induced velocity in the vertical direction, enhancing the growth rate on the bubble side.

Multi-mode RTI growth: role of internal dynamics

- **DNS with specific perturbation spectra reproduce the higher alpha seen in many experiments. These high values appear to be due either or both of** (this is also supported by the experiments of Carles et al 2006; Olson and Jacobs 2009):
  - too short an experimental time or
  - significant low wave number content in the IC.
- **Considerations on the confined RTI problem:**
  - RTI is relatively inefficient at converting potential energy into vertical kinetic energy; the growth rate coefficient, alpha, is much lower than that corresponding to free fall.
  - Vertical ejections, which are associated to induced vortical velocities, can convert back horizontal kinetic energy into vertical kinetic energy and increase the value of alpha.
  - Confined RTI, especially with a perturbation spectrum of the type k^{-3}, is just "single-mode RTI with noise." Enhanced vertical ejections activity is expected due to the specific alignement between vorticity and principal axes, along with higher growth rates.
- **At high A, the vorticity alignment with the principal axes also enhances the growth rate on the spike side.**

Mixing Layer Asymmetry

- **Mean density is self-similar:**
  - When scaled by the layer width, density profiles collapse to a profile that is constant in time.
- **Fixed point at z_0=0: $\langle\rho\rangle(z_0)$ is constant in time.**
- **Mean continuity equation:** $\frac{\partial}{\partial t}\langle\rho\rangle + \left(\langle\rho\rangle\tilde{U}_3\right)_{,3} = 0$ **. Thus** $\langle\rho\rangle\tilde{U}_3$ **peaks at z_0=0.**
- **Density is not symmetric. Thus velocity is not symmetric.**

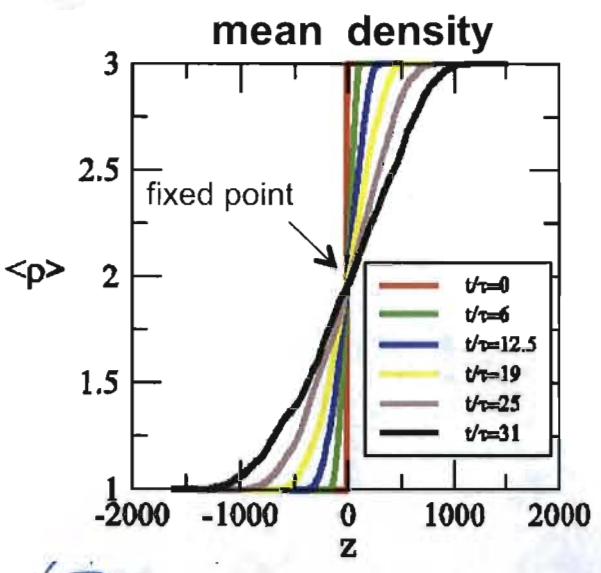

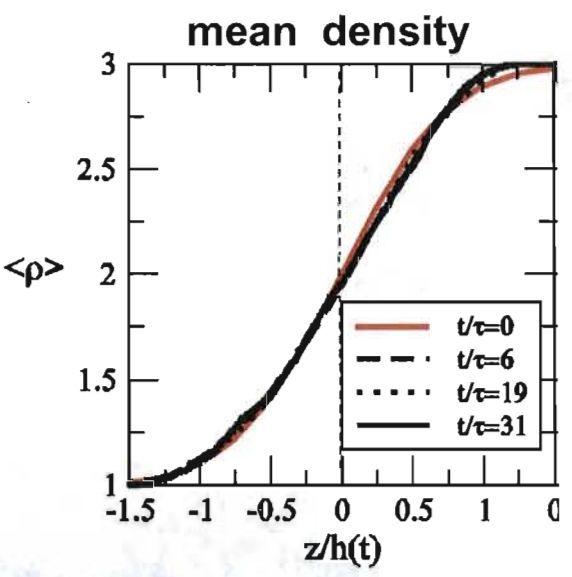

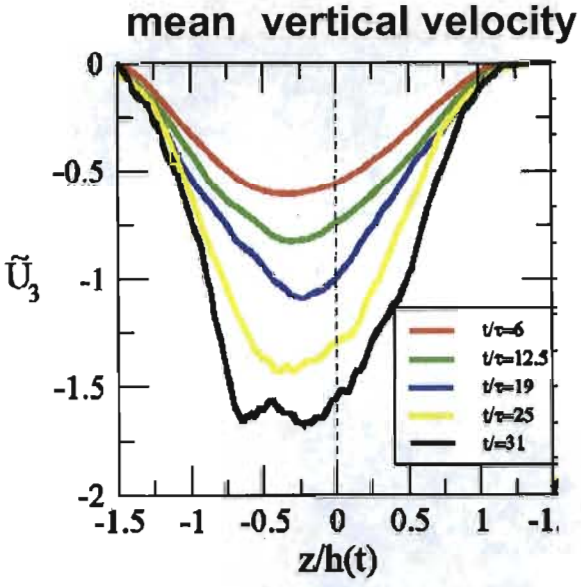

Turbulent kinetic energy transport equation budget

$$\frac{\partial}{\partial t}\left(\langle\rho\rangle\tilde{k}\right) = \underbrace{-\left(\langle\rho\rangle\tilde{U}_3\tilde{k}\right)_{,3}}_{I} \underbrace{+a_3 P_{,3}}_{II} \underbrace{-R_{33}\tilde{U}_{3,3}}_{III} \underbrace{-a_3\left\langle\tau_{33}\right\rangle_{,3}}_{IV} \underbrace{-\frac{1}{2}R_{ii3,3}}_{V} \underbrace{-\left\langle u_3' p'\right\rangle_{,3}}_{VI} \underbrace{+\left\langle u_i'\tau_{i3}\right\rangle_{,3}}_{VII} \underbrace{+\left\langle p' d'\right\rangle}_{VIII} \underbrace{-\left\langle\tau_{ij}u_{i,j}\right\rangle}_{IX}$$

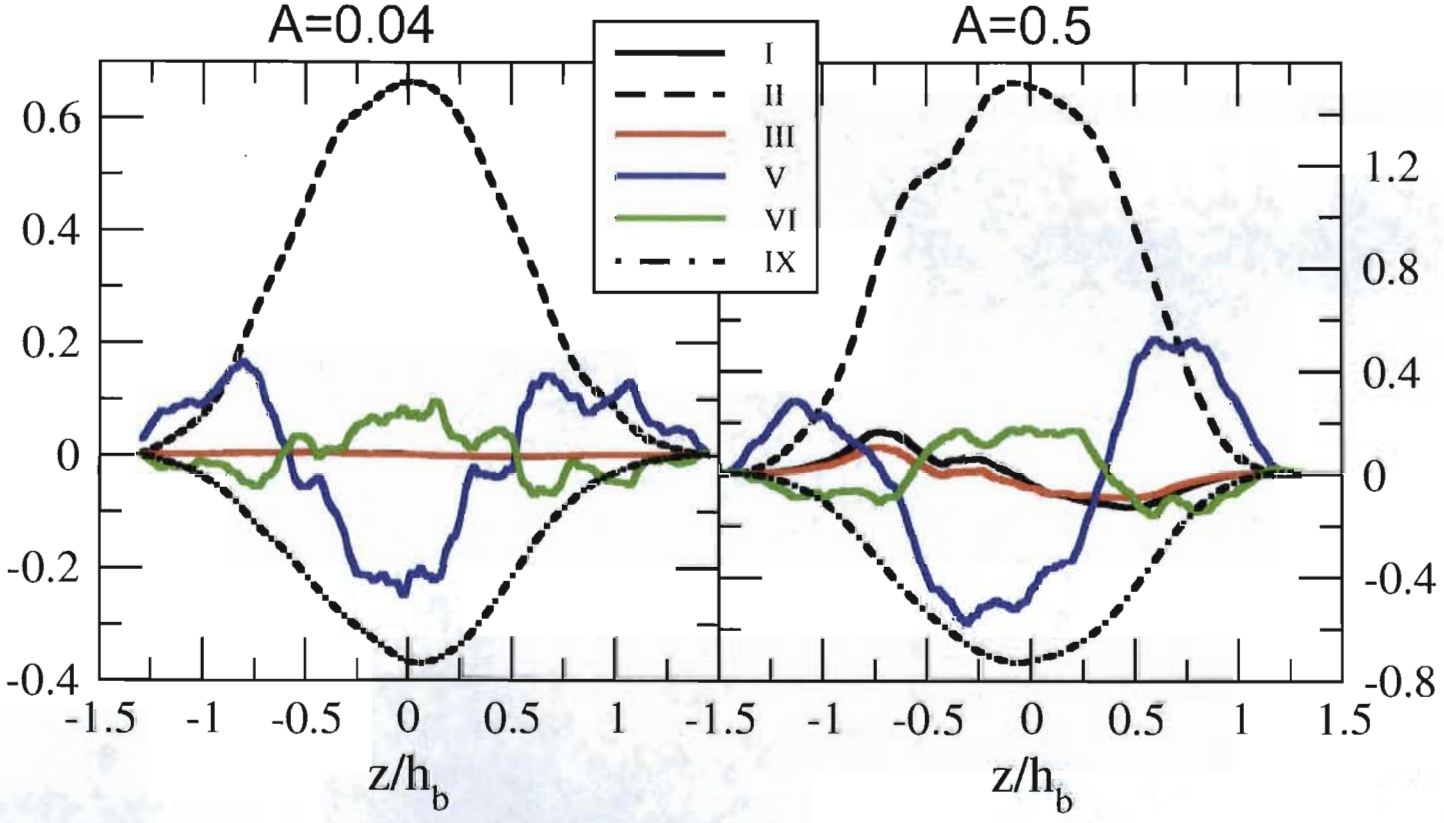

Turbulent kinetic energy transport equation budget

$$\frac{\partial}{\partial t}\left(\langle\rho\rangle\tilde{k}\right) = \underbrace{-\left(\langle\rho\rangle\tilde{U}_3\tilde{k}\right)_{,3}}_{I} \underbrace{+a_3 P_{,3}}_{II} \underbrace{-R_{33}\tilde{U}_{3,3}}_{III} \underbrace{-a_3\left\langle\tau_{33}\right\rangle_{,3}}_{IV} \underbrace{-\frac{1}{2}R_{ii3,3}}_{V} \underbrace{-\left\langle u_3' p'\right\rangle_{,3}}_{VI} \underbrace{+\left\langle u_i'\tau_{i3}\right\rangle_{,3}}_{VII} \underbrace{+\left\langle p' d'\right\rangle}_{VIII} \underbrace{-\left\langle\tau_{ij}u_{i,j}\right\rangle}_{IX}$$

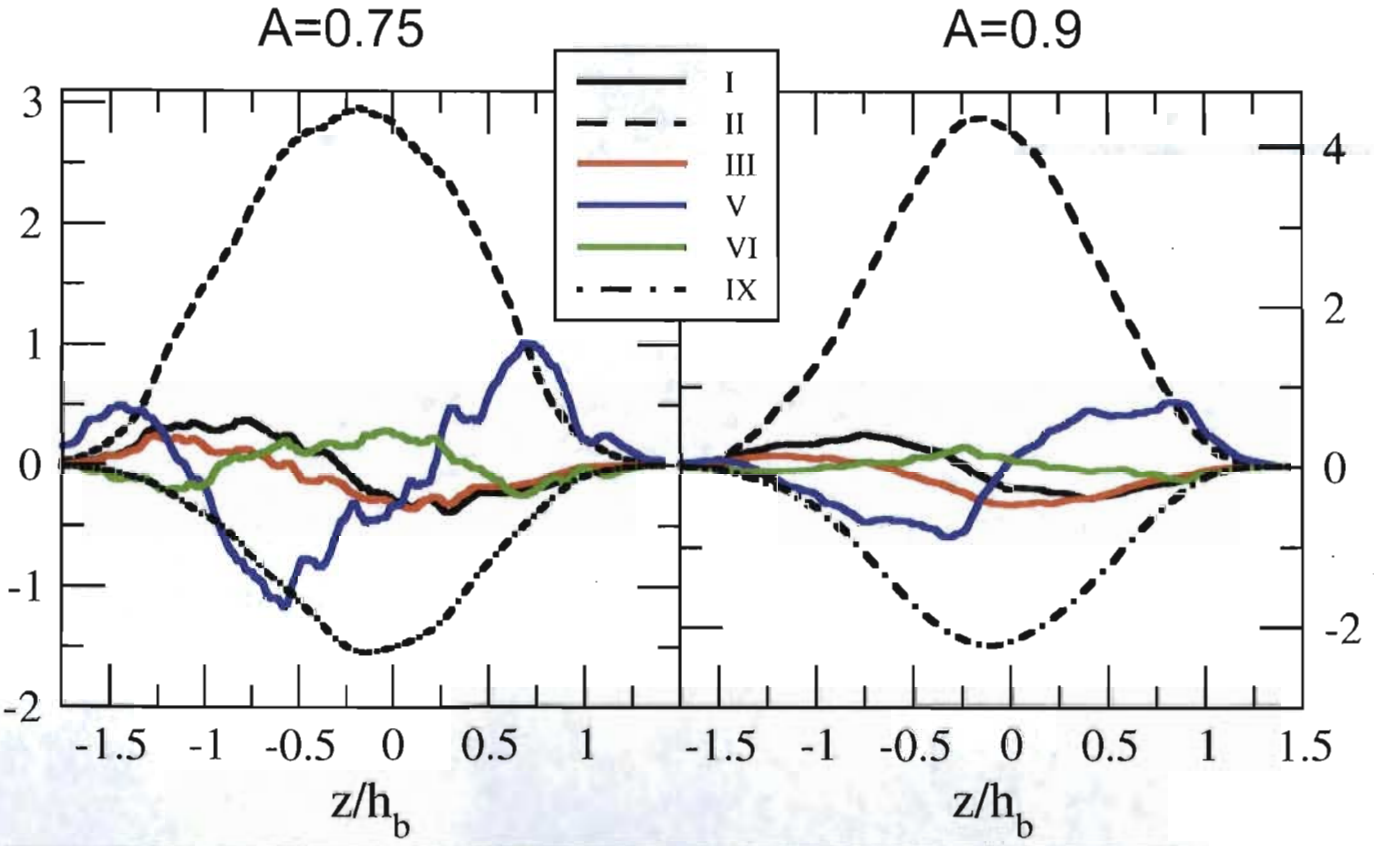

Spectra from 4096² x 4032 Rayleigh-Taylor at A=0.75

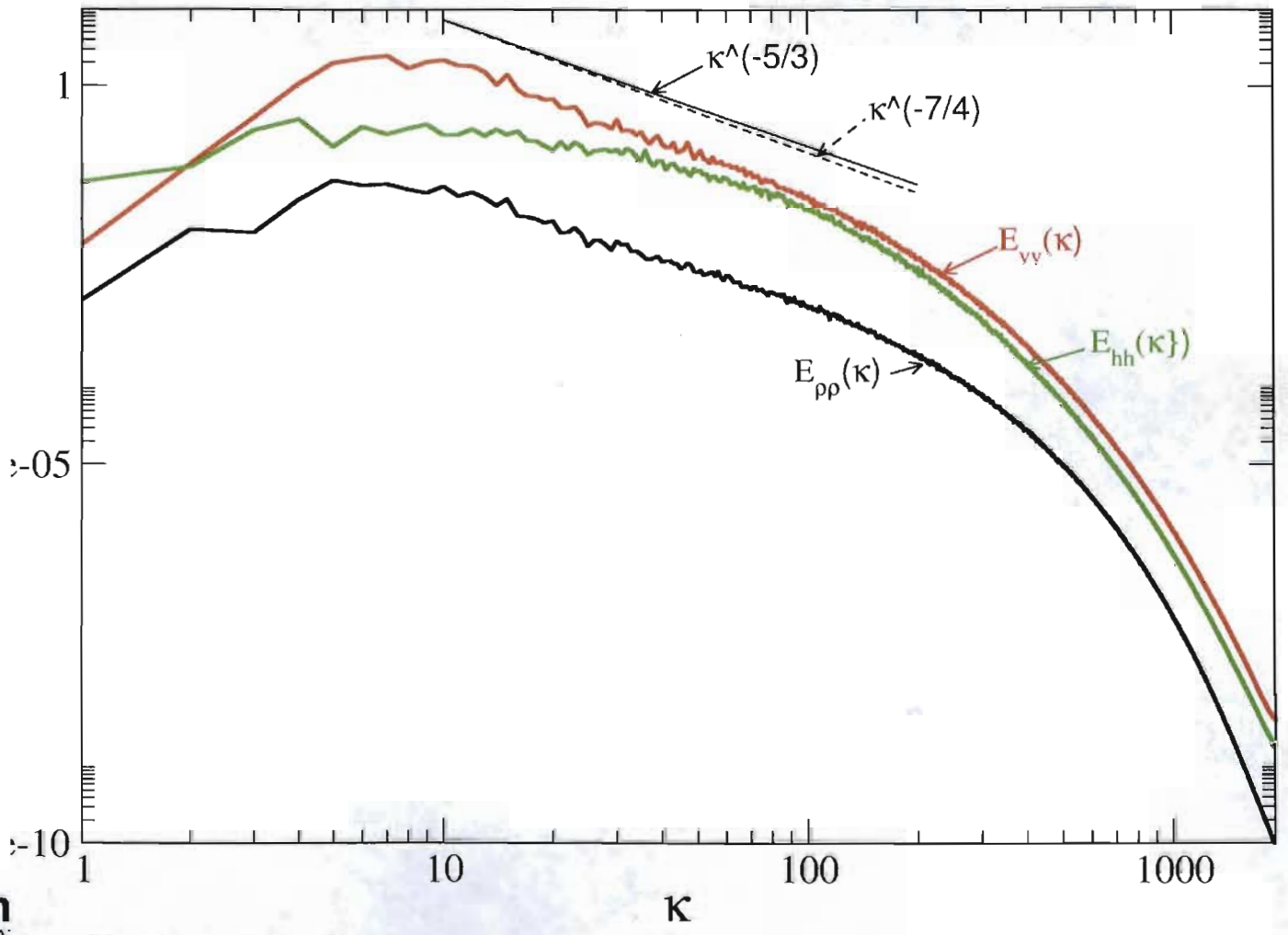

Normal stresses anisotropy

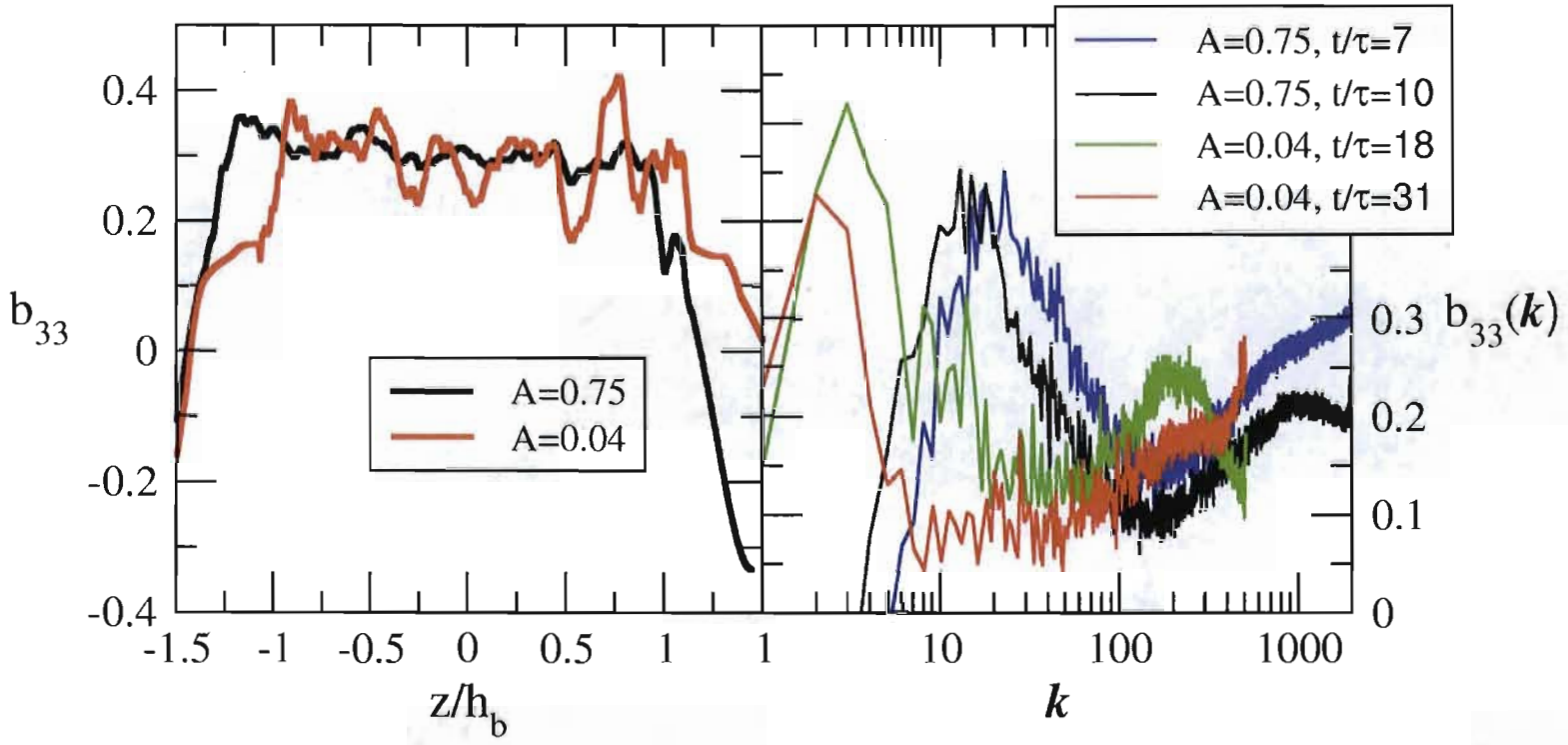

Mixing of pure fluids in homogeneous Rayleigh-Taylor turbulence

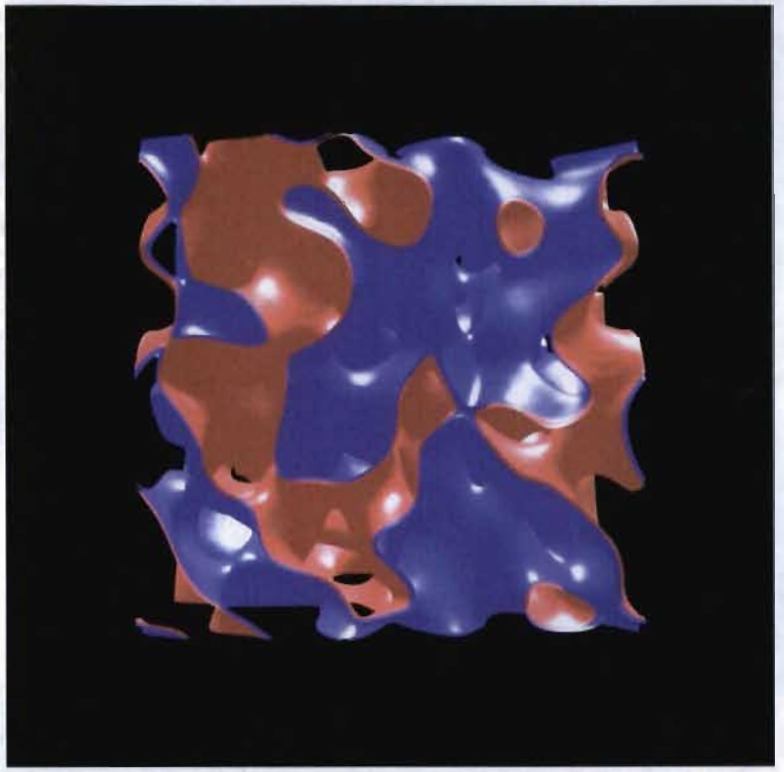

- **In variable density turbulence, mixing is asymmetric, with the pure heavy fluid mixing slower than the pure light fluid** (Livescu and Ristorcelli, J. Fluid Mech. 2008).
- **The mixing rate depends on the relative alignment between the density gradient and the principal directions, which is responds differently to the inertia of the two fluids.**

Density PDF and density surface density function across the Rayleigh-Taylor layer at A=0.75

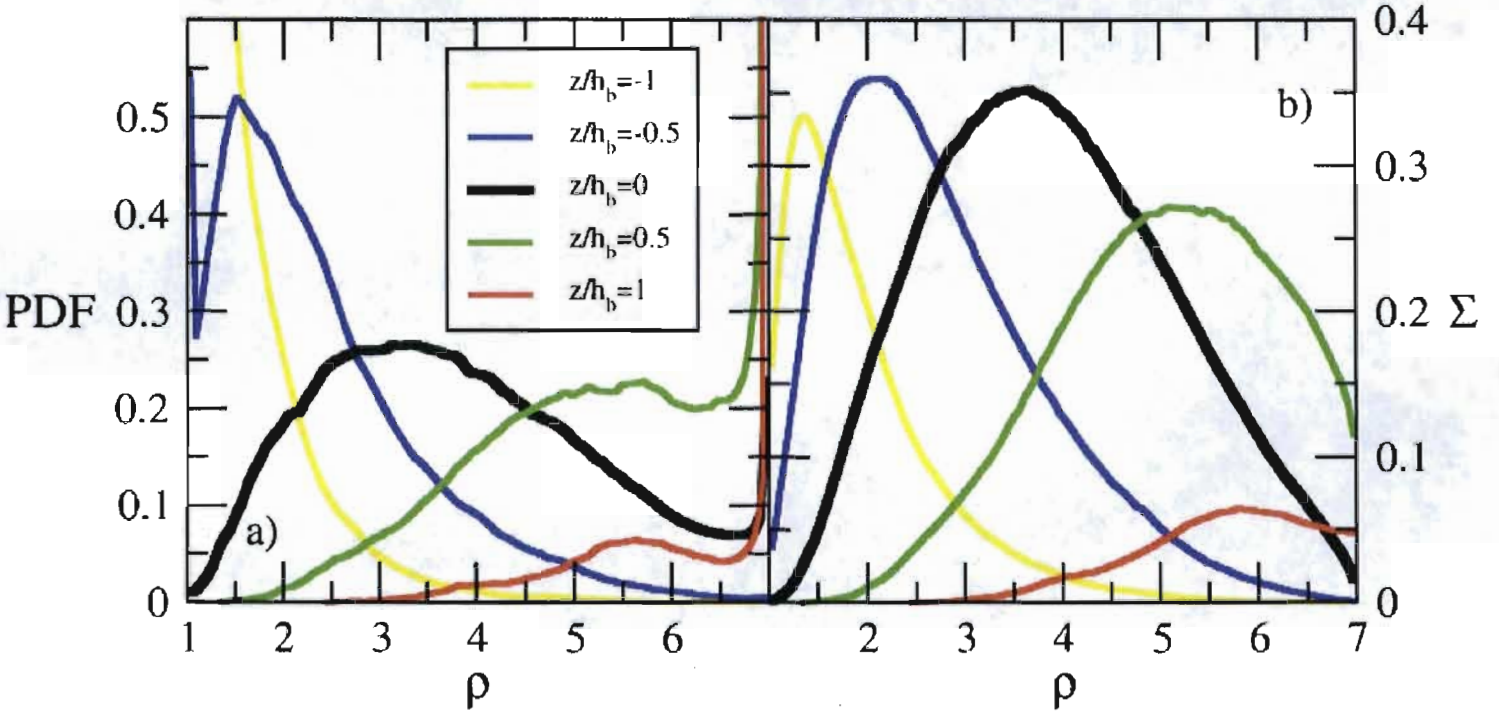

- Density PDF is asymmetric with respect to the centerline → **Larger penetration distance of the pure heavy fluid.**
- Density surface density function shows more fragmentation on the light fluid side → **The edges of the layer differentiate into spikes and bubbles.**

Mix metrics used in Rayleigh-Taylor turbulence

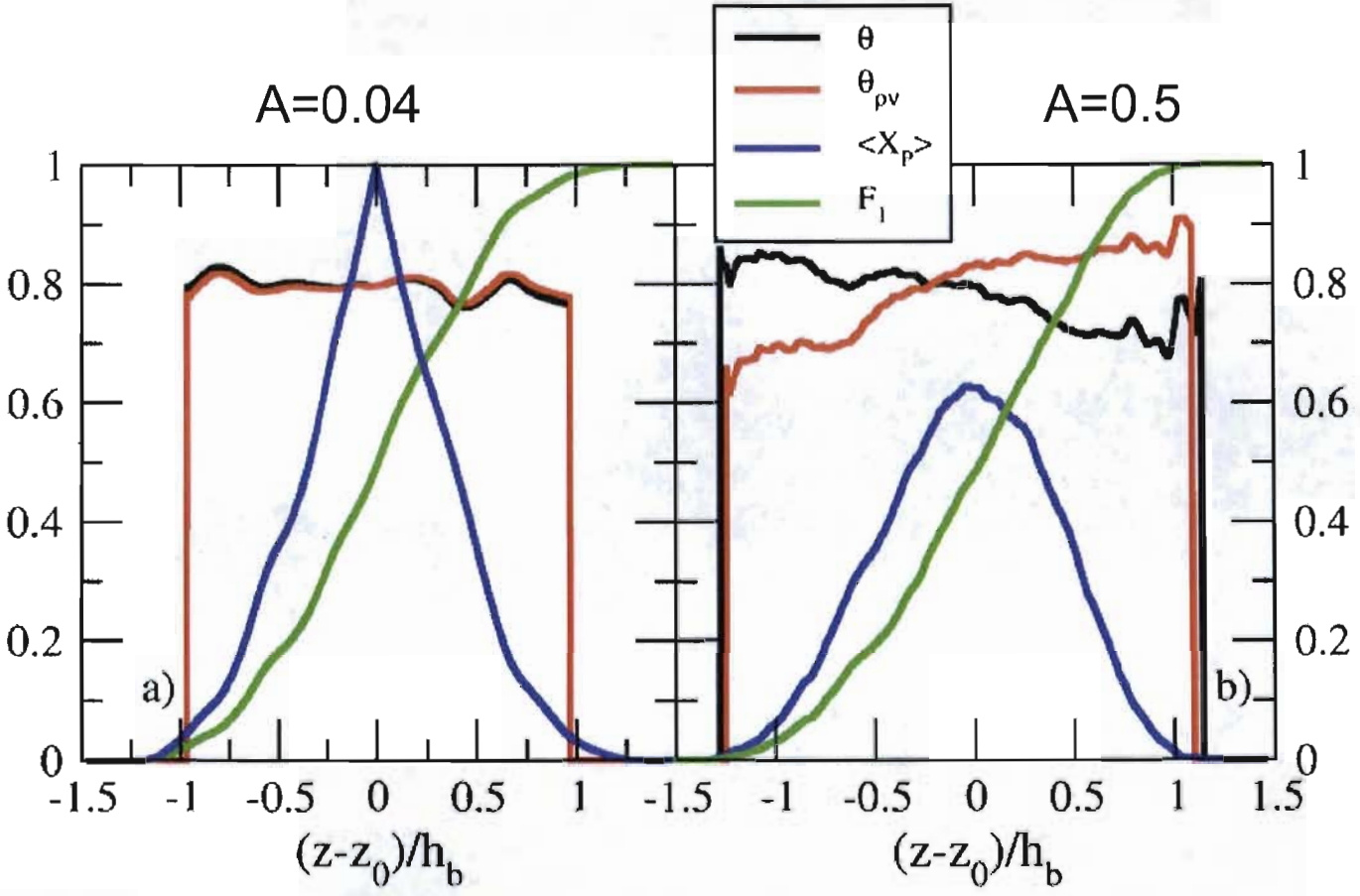

Mix metrics used in Rayleigh-Taylor turbulence

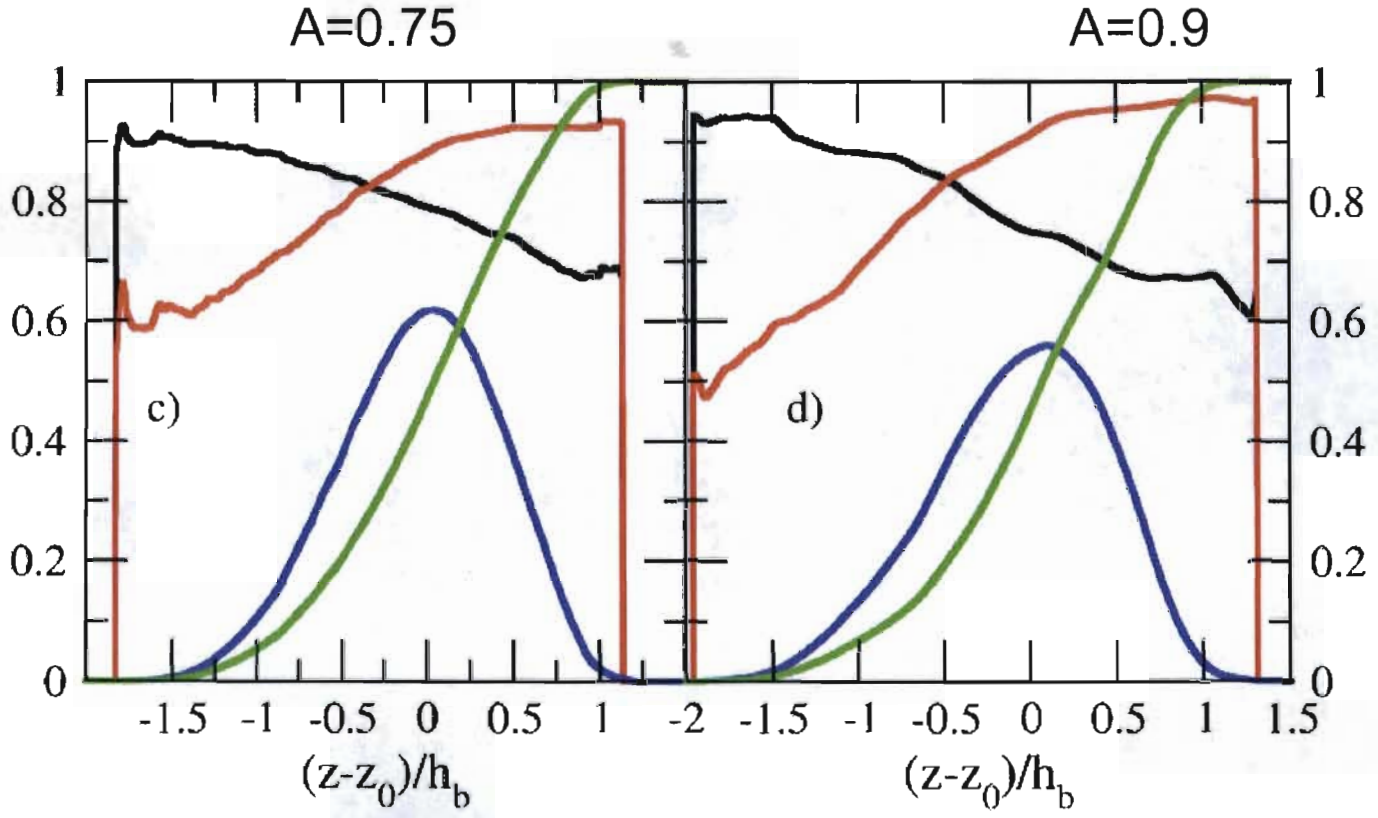

Summary and Conclusions

- Turbulence and mixing characteristics in non-Boussinesq turbulence were examined using Direct Numerical Simulations from a new set of simulations with A=0.04, 0.5, 0.75, 0.9 on $1024^2 \times 4032$ and $4096^2 \times 4032$ meshes
- The layer width reaches self-similarity for all cases, with $a_b \approx 0.025$ (the value changes slightly with the Atwood number), for all initial perturbation spectra and all viscosities and diffusivities examined provided that the turbulent structures can grow laterally unrestricted (no interaction with the walls).
- Laterally confined RTI can grow faster due to restrictions in the vortical motions, which lead to a specific alignment between vorticity and principal axes.
- Mixing asymmetry changes the shapes of the two edges of the layer. On the spike side the specific alignment between vorticity and principal axes leads to faster growth.
- The density and velocity spectra develop inertial ranges; within the inertial ranges, the flow becomes close to isotropic, however there is a persistent anisotropy at small scales.

Considerations on the transition to turbulence and the time when a turbulence model can be used for multi-mode RTI

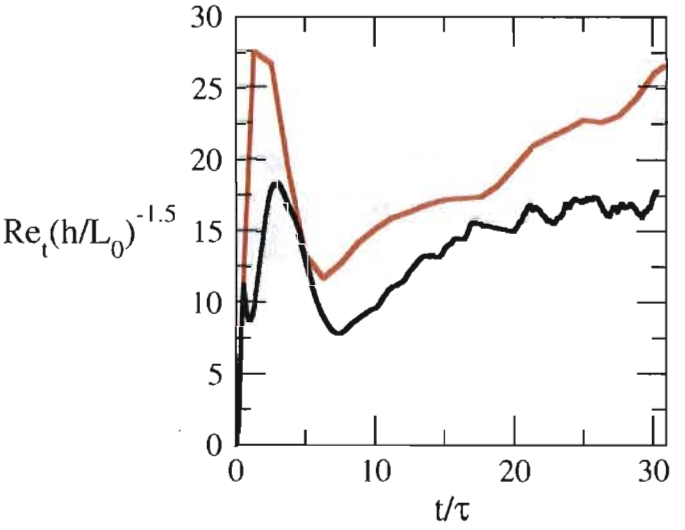

- Although the layer width becomes self-similar relatively fast, derived quantities, such as the turbulent Reynolds number, in general, require longer time to reach self-similarity.
- Since Re_t is proportional to the eddy viscosity in the usual gradient transport model, this suggests such a model becomes applicable later than the onset time for layer self-similarity.

Spectra from 4096^2 x 4032 Rayleigh-Taylor at A=0.75

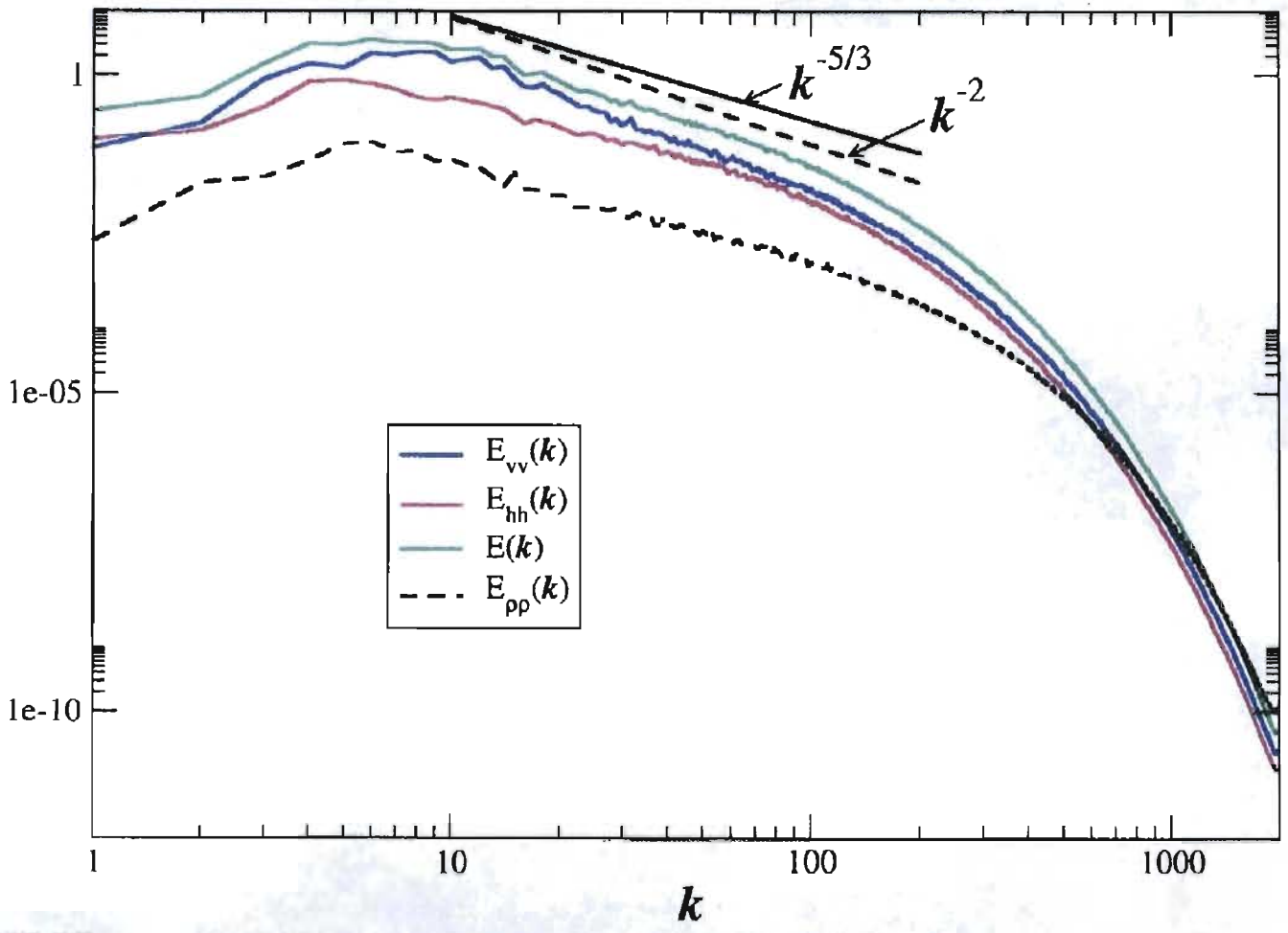

Q-R from 4096^2 x 4032 Rayleigh-Taylor at A=0.75